Fuel Processing Technology 276 (2025) 108270

Contents lists available at ScienceDirect

Fuel Processing Technology

journal homepage: www.elsevier.com/locate/fuproc

Research article

Kinetic investigation of NH_3 decomposition over Ru-based catalysts: The limiting role of H* surface coverage and its impact on reactor engineering

Yi Qiu, Federico Sascha Franchi, Nicola Usberti, Alessandra Beretta *

Laboratory of Catalysis and Catalytic Processes, Dipartimento di Energia, Politecnico di Milano, via La Masa 34, 20156 Milano, Italy

ARTICLE INFO

Keywords:
NH_3 decomposition
$Ru/MgAl_2O_4$
$Ru/\gamma\text{-}Al_2O_3$
Ru/MgO
Kinetic model
Reactor design

ABSTRACT

H_2 production via green NH_3 decomposition is a key process in the value chain of renewable energy storage and distribution, but reactor engineering studies are at an early stage due to the still open research on catalyst formulation and reaction kinetics. In this work, the kinetics of NH_3 decomposition are studied over $Ru/MgAl_2O_4$, $Ru/\gamma\text{-}Al_2O_3$ and Ru/MgO catalysts, that combine the best-known active metal, Ru, and supports suitable for industrial applications. For all the formulations, NH_3 concentration and H_2-cofeed are found to negatively affect the conversion, in line with the literature; however, original experiments at varying NH_3 concentration with large H_2-cofeed unambiguously show that, in the presence of H_2-rich streams representative of the catalyst application, the intrinsic kinetics have a linear dependence on NH_3 partial pressure and a negative order (−1.5) with respect to H_2 partial pressure, consistent with the hypothesis that ammonia dehydrogenation is rate determining and H* is the most abundant surface intermediate. The same kinetic dependences were obtained over a commercial Ru-based catalyst. The kinetic relevance of hydrogen coverage and the intrinsic first order dependence on NH_3 have two important implications: on a methodological plane, the performance and kinetics of the catalyst under industrially relevant conditions (e.g. pure ammonia) can be captured even under highly diluted NH_3 feeds (which guarantee the rigorous isothermal conditions) provided that the large H_2 contents are experienced; on a more applicative plane, both kinetic and thermodynamic factors play negatively at increasing concentration and pressure, thus large sizing (with GHSV values as low as 2500 Nl/kg/h) is needed to obtain complete ammonia conversion below 500 °C.

1. Introduction

To achieve net-zero CO_2 emissions in the coming decades, green hydrogen is considered as one of the most promising energy carriers for future energy systems [1]. To overcome the challenges for the storage and transportation of hydrogen, a practical alternative is to chemically convert it into high density hydrogen carriers, from which H_2 can be re-obtained by dehydrogenation or decomposition processes [2]. Among them, NH_3 has outstanding features: (i) NH_3 has high volumetric density (108 kg-H_2/m^3 NH_3 at 20 °C and 8.6 bar) and gravimetric density (17.8 wt%) of hydrogen; (ii) it is a chemical commodity with well-established technologies of production (based on the Haber-Bosch process) as well as developed infrastructures of storage and transportation [3]; (iii) H_2 and N_2 are the only products from NH_3 decomposition, while C-products (CO, CO_2, CH_4, coke) are expected from the decomposition or dehydrogenation of other liquid H_2 carriers [4]. Despite the highly favorable features, the development of a large-scale value chain of NH_3 synthesis, transport and decomposition still presents open issues. Safety and environmental issues are raised by ammonia toxicity; however, important progresses in the safe transfer and bunkering of ammonia have been recently announced, which makes realistic the short-term realization of large ammonia hubs in Northern Europe [5].

Besides, ammonia decomposition is still an immature technology, which is currently one of the most important limitations in the use of ammonia as an energy carrier [6]; H2Retake™ by TOPSOE is one of the few commercially proven ammonia cracking technology [7]. The identified open areas of research include catalysis development, H_2 purification methods and reactor design.

Several studies have explored catalyst formulations for ammonia decomposition. Ganley et al. systematically studied a wide series of transition metals in ammonia decomposition and reported their activity in decreasing order as Ru > Ni > Rh > Co > Ir > Fe > Pt > Cr > Pd > Cu > > Te, Se, Pb [8]. Similar scale of reactivity was obtained in later works and documented by recent reviews [9,10].

* Corresponding author.
E-mail address: alessandra.beretta@polimi.it (A. Beretta).

https://doi.org/10.1016/j.fuproc.2025.108270
Received 12 March 2025; Received in revised form 4 June 2025; Accepted 12 June 2025
Available online 20 June 2025

Ammonia decomposition reaction has been recognized as structure sensitive with B5 sites as mostly active over Ru-based catalysts; the concentration of such sites and turnover rates have been found to depend on the Ru cluster size and shape based on experimental and theoretical approaches [11,12]. Similarly, the activity has also been found to be affected by the nature of the support. It was reported that the supports of Ru catalyst for NH_3 decomposition should concomitantly possess the following properties: basicity, conductivity, low concentration of electron-withdrawing groups, high thermal stability, and high surface area (for good dispersion of active metals) [13,14]. Wide reports on the use of Al_2O_3, MgO and $MgAl_2O_4$ are found in the literature [15–19].

The following set of elementary reactions has been typically assumed in the literature, starting from the historical studies aiming at better understanding ammonia synthesis [20,21] to the more recent kinetic, microkinetic and DFT studies for ammonia decomposition [22–24].

Step 1 - NH_3 adsorption $NH_3 + * \leftrightarrow NH_3*$

Step 2 - First N—H cleavage $NH_3* + * \leftrightarrow NH_2* + H*$

Step 3 - Second N—H cleavage $NH_2* + * \leftrightarrow NH* + H*$

Step 4 - Third N—H cleavage $NH* + * \leftrightarrow N* + H*$

Step 5 - N_2 desorption $N* + N* \leftrightarrow N_2 + 2*$

Step 6 - H_2 desorption $H* + H* \leftrightarrow H_2 + 2*$

Different interpretations on the nature of the rate-determining step (RDS) have been given in the literature. Based on microkinetic modelling combined with density functional studies, Hansgen et al. [25] concluded that the heat of nitrogen chemisorption is a good descriptor to identify surfaces with desirable catalytic activity for ammonia decomposition. The binding energy of the nitrogen atom to the surface must be strong enough for dehydrogenation of the NH_X species to occur, but sufficiently weak so that the recombined nitrogen could desorb from the surface. This trade-off leads to a volcano-type relationship between nitrogen binding energy and turnover rate, with maximum at 125 kcal/mol. Ru would lie close to the volcano peak, where the reaction is predicted to be sensitive to the rupture of the second N—H bond (step 3 above), and less sensitive to the recombination of N* species.

Very scattered reports are found in the literature from experimental studies while a comprehensive review has been provided by Su et al. [26]. By investigating ammonia decomposition on a series of metals, Logan and Kemball provided evidence that the RDS for all the catalysts tested (Ni, Co, Rh, Pt, Ru, Re, Fe, V, and W) was the desorption of nitrogen [27]. Combining experimental data with kinetic modelling, Takahashi et al. concluded that the RDS for Ru/MgO catalyst was nitrogen desorption, whereas for Ni/MgO catalyst it was within the dehydrogenation pathway of ammonia [28]. Fang et al. proposed that at low to mild temperatures the RDS is the recombination of N atoms, while it may switch to the N—H cleavage at high temperatures [29]. Ganley et al. [8] concluded that the nature of the rate-determining step was different on different catalysts, being the recombination of N* over non-noble metals, and the dehydrogenation of NH_3 on noble metals.

A large variability of measured turnover rates and of the mechanistic proposals is thus reported in the literature; it is believed that the scatter among experimental evidence can be associated with important effects, of metal-support interactions [30], promoters [31,32], shape and size of Ru aggregates; besides, a factor of complexity is given by the kinetic behavior that, as well shown in this study, determines a large sensitivity of the catalyst performance (i.e. the measured ammonia conversion) versus the gas-phase composition. Finally, given the endothermic nature of the reaction, the use of concentrated ammonia feed (as desirable to align the experimental study to the final application) puts the kinetic investigation at the risk of axial and radial temperature gradients across the catalyst bed, which may represent a fatal bias in the kinetic investigation, preventing the correct interpretation of data and the development of reliable kinetic models.

Starting from extensive reports on the activity data among a wide variety of Ru-based formulations [33,34], in this work, focus is put on a narrow selection of catalysts (Ru/γ-Al_2O_3, Ru/MgO and Ru/$MgAl_2O_4$) aiming at a comparative analysis of the main kinetic dependences, which requires the adoption of common and kinetically relevant conditions. The three selected supports are all well-established materials for industrial scale applications and are thus suitable materials for addressing preliminary reactor calculations; it is in fact of great interest to understand if not only the activity but also the kinetics are quantitatively and qualitatively affected by the nature of the support. Kinetically controlled conditions were guaranteed by using highly diluted feeds which allow to rigorously compare the performance of the various formulations and to investigate the effects of the main operating conditions (temperature, feed composition) aiming at the identification of the prevailing kinetic dependences. This preliminary engineering analysis allows on one side to critically evaluate the representativeness of the lab-scale investigation (especially with reference to the feed composition), on the other side to identify strategies for the catalyst optimization and reactor design to meet the industrial needs.

2. Materials and methods

2.1. Catalyst preparation

Ru-based catalysts were prepared via incipient wetness impregnation (IWI) method. $Ru(NO)(NO_3)_3$ (Alfa Aesar, 1.5 %g_{Ru}/ml) was used as precursors of the active phase. Three commercial supports were used, namely γ-Al_2O_3 (Sasol PURALOX SCFa140/L3), MgO (ALDRICH) and $MgAl_2O_4$ (Sasol PURALOX MG28/100, a spinel phase mixture of 28 % MgO + 72 % Al_2O_3).

The supports were first calcined at 500 °C for 5 h in air (temperature ramp: from room temperature to 500 °C with a rate of 1 °C/min, held at 500 °C for 5 h, then ramp down to room temperature with a rate of 2 °C/min). The impregnation was then performed by adding the solution of Ru precursor to the supports powder drop by drop. Ru concentration in the impregnating solution was set to obtain a nominal metal loading of 1 wt%. According to the pore volume of different supports, impregnations were performed twice on γ-Al_2O_3 and $MgAl_2O_4$, while for MgO four consecutive impregnations were needed. After impregnation, the catalysts were dried at 125 °C in air overnight. The prepared catalysts Ru/γ-Al_2O_3, Ru/MgO and Ru/$MgAl_2O_4$ are hereafter referred to as RuA, RuM and RuMA, respectively.

2.2. Catalyst characterization

Morphological properties were measured by N_2-adsorption/desorption using a Micromeritics Tristar 3000 instrument. Prior to the analysis, each sample was degassed at 120 °C for 3 h.

Ru dispersion was estimated by CO pulse-chemisorption using a TPD/R/O 1100 Thermo Fischer Instrument. The sample was pre-treated with an initial reduction, carried out by flowing 5 % H_2/Ar (20 Nml/min) and heating from room temperature up to 450 °C (5 °C/min); after a hold at 450 °C for 1 h, the sample was cooled down to 30 °C in He and then exposed to successive pulses which contained 0.924 ml of a 4.99 % CO in He mixture. The series consisted typically of 20–25 pulses, until reaching of a steady-state train of peaks at the TCD detector.

The microstructures of catalysts were observed by scanning electron microscopy (SEM), using a Zeiss Evo 50 with EDS Bruker Quantax 200 6/30 probe instrumentation.

Transmission electron microscopy (TEM) study was performed using a double-corrected JEOL ARM 200F instrument in STEM (scanning transmission electron microscopy) mode to analyze Ru nanoparticles.

CO_2 Temperature-Programmed Desorption (CO_2-TPD) was performed to evaluate the basicity of the catalysts. Prior to analysis, the catalysts were reduced under 1 % H_2. Subsequently, a gas mixture containing 2 % CO_2, 10 % N_2, and 88 % He was introduced to the sample at room temperature for 1 h to allow for CO_2 adsorption. Following this, CO_2 flow was halted, and the sample was purged with a mixture of 10 % N_2 and 90 % He for an additional hour. The temperature was then

ramped to 600 °C at a rate of 10 °C/min. Desorbed CO_2 was monitored using a gas chromatograph (GC).

Ammonia temperature-programmed desorption (NH_3-TPD) was carried out over the three catalysts and the γ-Al_2O_3 support, using the testing rig and reactors as for the activity tests. Before measurement, He was fed to the reactor at 350 °C to clean the catalyst surface then the sample was cooled down to 150 °C. At this temperature, 1 % NH_3/He was fed to the reactor. After the adsorption, the flow was switched to pure He. Then TPD procedure started from 150 °C to 450 °C at a rate of 5 °C/min and held at 450 °C for 1 h. With the same setup, hydrogen/nitrogen temperature programmed desorption (H_2 or N_2-TPD) were also conducted. The samples were exposed to a 1 % H_2/He or 1 % N_2/He stream for 1 h at 350 °C; afterwards, the gas was switched to pure He while cooling down to 50 °C. After stabilization, the temperature program started from 50 °C to 450 °C, with a rate of 5 °C/min, and a final hold at 450 °C for 1 h.

2.3. Activity tests

Ammonia decomposition tests were performed in a micro fixed-bed quart tube reactor with an internal diameter of 9 mm. Typically, a bed of 300 mg of catalyst diluted with 150 mg quartz powder (mesh 140–200, corresponding to 75–106 μm particle size) was loaded in the quartz tube in between layers of pressed quartz wools. The reactor was placed in the isothermal zone of an electric tubular furnace and the temperature was controlled by a K-type thermocouple placed in the middle of the catalyst bed. A Pfeiffer Vacuum ThermoStar mass spectrometer was connected to the outlet of the reactor to continuously analyze the products.

Cylinders of 2.55 % NH_3 with 0.506 % Ar as tracer in He, 5.03 % H_2 in Ar, pure H_2 and pure N_2 were connected to the experiment rig. Prior to the reaction, the catalyst was pretreated at 450 °C under 1 %H_2/He flow for 1 h. The procedure was based on in-house experience also with commercial catalysts and intended to obtain the decomposition of the Ru precursor and reduction of the noble metal into stable aggregates.

All the activity tests were conducted in the temperature range of 240–500 °C, at the gas hourly space velocity GHSV of 20,000 Nl/Kg_{cat}/h, under atmospheric pressure; to preserve the isothermal conditions, experiments were performed with He-diluted feed steams. The effect of NH_3-inlet concentration on the reaction kinetics was measured in the range 0.3 % to 2.55 %. Tests were then performed by cofeeding the reaction products (H_2 and N_2) while keeping NH_3 at 0.3 %/1 %. H_2 cofeed was explored in the range 1 %–25 %, while N_2 cofeed was tested with 10 % N_2. Replicated experiments under reference conditions (1 %/0.3 % NH_3 in He) were periodically performed and guaranteed the substantial stability of the catalyst performance.

Based on replicated experiments, we can estimate that the experimental error on the measure of ammonia conversion is within ±3 %.

2.4. Reactor modelling

The packed-bed reactor was modelled by a 1D isothermal and isobaric pseudo-homogeneous model, consisting of the differential mass balances for NH_3, H_2, N_2 (Eq. (1)) with initial conditions (2) as follows.

$$\frac{dF_i}{dW_{CAT}} = \nu_i \bullet r_{NH_3} \bullet \left(1 - \frac{K_P}{K_{Eq}}\right) \tag{1}$$

$$W_{CAT} = 0; F_i = F_{i,0} \tag{2}$$

where F_i and $F_{i,0}$ are the molar flows of the generic species i ($i = NH_3, H_2, N_2$, [mol/s]) along the reactor axis and at the reactor inlet, respectively, W_{CAT} is the catalyst load [g_{CAT}], ν_i the stoichiometric coefficient of the i^{th} species, and r_{NH_3} is the forward ammonia decomposition rate [mol/s/g_{CAT}]. The negligible role of temperature and concentration gradients at the bed, gas-solid interface and particle scales was supported by the application of conventional *a-posteriori* verification criteria (summarized in [35]) and easily justified by the relatively moderate observed reaction rates, the small particle size, the bed-dilution, the very limited power demand.

The term $\left(1 - \frac{K_P}{K_{Eq}}\right)$ accounts for the approach to thermodynamic equilibrium, being $\frac{K_P}{K_{Eq}}$ the ration between the reaction quotient and the equilibrium constant at a given temperature. The temperature dependence of the equilibrium constant K_{Eq} was taken from ref. 36 and calculated as:

$$K_{Eq} = (K_A K_B)^{-1} \tag{3}$$

$$\log_{10}(K_A) = \left(0.1191849 * T^{-1} + 91.87212 * T^{-2} + 2.512273 * 10^7 * T^{-4}\right) * P \tag{4}$$

$$\log_{10}(K_B) = -2.691122 * \log_{10}(T) - 5.519265 * 10^{-5} * T + 1.848863 * 10^{-7} * T^2 + +2001.6 * T^{-1} + 2.6899 \tag{5}$$

The total molar flow F_{TOT} includes the flow of the inert species (He) that in the case of simulation of the highly diluted experiments prevails over the flows of reacting species, such that F_{TOT} can be assumed constant across the bed; however, to account for cases of more relevant effects of the reaction stoichiometry on the total molar flow, the additional equation was also incorporated:

$$\frac{dF_{TOT}}{dW_{CAT}} = \sum_i^{NS} \nu_i \bullet r_{NH_3} \bullet \left(1 - \frac{K_P}{K_{Eq}}\right) = r_{NH_3} \bullet \left(1 - \frac{K_P}{K_{Eq}}\right) \tag{6}$$

with $F_{TOT} = F_{NH3} + F_{N2} + F_{H2} + F_{He}$ [mol/s].

The differential system constituted by the mass balance equations was integrated numerically with the Fortran subroutine LSODI which allows to solve stiff problems using Gear's implicit integration method with variable steps. The kinetic parameters were estimated by nonlinear regression, performed using the Fortran subroutine BURENL based on the least-squares method.

3. Results and discussion

3.1. Characterization

The three supports used in this study have largely different morphological properties.

Table 1 lists the measured BET surface area, pore volume and average pore size of the catalysts after impregnation. The morphological properties of the starting supports are reported in the Supplementary Material (Table S1). Notably RuM is characterized by poorer morphological properties, with surface area and pore volume that are significantly lower than those of the other two systems.

The dispersion of the metal was investigated by CO pulse chemisorption. The results are reported in Table 1 in terms of CO/Ru ratio. Assuming a 1 to 1 stoichiometry of adsorption [38], thus taking the CO/Ru ratio as a measure of metal dispersion, the estimated mean Ru size is

Table 1
Ru-catalysts characterization.

Name	BET Surface Area (m^2/g)	Pore Volume (cm^3/g)	Pore diameter (Å)	CO/Ru	d_{Ru}* (nm)
RuA	180	0.37	56	0.72	1.8
RuM	14	0.09	253	0.47	2.7
RuMA	113	0.39	94	0.99	1.3

*Calculated from CO pulses chemisorption, using equation $d_{Ru} = 6 * \frac{\nu_{Ru}/a_{Ru}}{d_{VA}}$, with ν_{Ru}=13.65 Å^3, a_{Ru}=6.35 Å^2 [37].

1.8, 2.7, 1.3 nm for RuA, RuM, RuMA respectively.

SEM-EDX analyses (reported in the Supplementary Information in Fig. S1–S3) showed that Ru particles are present and uniformly distributed on the catalyst surface.

Figs. 1a–c report the High-Resolution Scanning Transmission Electron Microscopy (HR-STEM) images of the three catalysts. It is shown that Ru nanoparticles are present, exhibiting very small sizes. For RuM, the nanoparticles sizes mostly range between 0.5 and 2 nm, with an average size of 1.15 nm. RuMA shows nanoparticles ranging from 0.26 to 1 nm, with an average size of 0.75 nm. In both cases, the particle size measurement was conducted on 300 particles across 11 different regions of the catalyst sample. Interestingly, on RuMA nanoaggregates consisting of 3 × 3 Ru atoms can be clearly identified. In the case of RuA, carbon contamination hindered the clear identification and counting of Ru nanoparticles, preventing statistical analysis. Nevertheless, it is generally observable that Ru nanoparticles are still predominantly smaller than 2 nm.

3.2. Adsorption/desorption experiments

According to the electron donor–acceptor theory, basicity is a key property influencing catalytic activity in NH_3 decomposition [39]. The basicity of the investigated catalysts was evaluated using CO_2-TPD, and the corresponding desorption profiles are presented in Fig. 2. Desorption peaks are conventionally associated with weak (<200 °C), medium (200–450 °C) and strong (>450 °C) basicity [40]. It can be seen that RuMA has more weak basic sites than the other two samples, while RuM shows more strong basic sites. The total CO_2-adsorption capacity determined (Table S2) decreases in the following order: RuMA> RuM> RuA.

NH_3-TPD tests were performed to evaluate the NH_3 adsorption capacity and capture the onset temperature of NH_3 activation on Ru. The obtained NH_3 desorption curves are shown in Fig. 3.

In the case of RuM, as can be seen from Fig. 4a, no desorption of NH_3 was detected, thus the catalyst did not trap any appreciable amount of the reactant during the adsorption phase at 150 °C, which is in line with the basicity of the support. No appreciable H_2 and N_2 could be detected during the temperature ramp.

Instead, in the cases of RuMA (Fig. 4b) and RuA (Fig. 4c), NH_3 desorption was observed, consistently with the increasing acidity of the supports; N_2 and H_2 were also detected in the outlet stream, indicating the simultaneous occurrence of a decomposition reaction from the desorbing reactant. Interestingly, the onset of the gas phase evolution of H_2 lagged behind N_2 (about 196 °C vs 168 °C), suggesting a stronger retention of H_2 on the catalyst; both profiles, though, clearly show that ammonia decomposition can be activated by Ru at very low temperature. An analogous piece of evidence is deduced from the signals obtained from RuMA where however N_2 and H_2 were observed only in small traces. The quantification of each detected species can be seen in Table S3; the overall ammonia adsorption capacity can be estimated and decreases in this order: RuA > RuMA>RuM.

Interestingly, the same NH_3 adsorption capacity as RuA was measured over the bare γ-Al_2O_3 support, which suggests that NH_3 adsorption mostly occurs on the acid sites of the support.

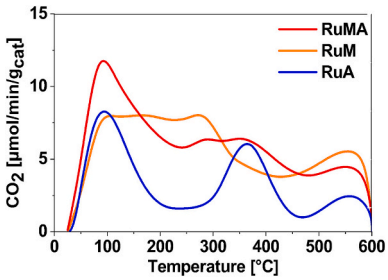

Fig. 2. CO_2 desorption over RuA, RuMA and RuM during CO_2-TPD.

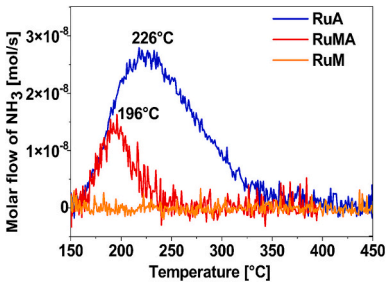

Fig. 3. Molar flow of NH_3 over RuA, RuMA and RuM during NH_3-TPD.

H_2-TPD experiments were also performed over the three catalysts. In analogy to the case of NH_3-TPD, the information that H_2-TPD provides is twofold: on one side the area of the desorption peak reveals the coverage of strongly adsorbed H* left from the dissociative adsorption of H_2 ($H_2 + 2^* \rightarrow 2H^*$) (Table S4), on the other side the temperature of desorption relates to the kinetics and energy of the associative desorption of H* (thus the reverse step $2H^* \rightarrow H_2$). Both quantities are indicators of the strength of the Ru—H bond. The results are presented in Fig. 5. The H_2 capacity and desorption temperature grew in the order: RuM < RuMA < RuA which suggests an increasing trend of the Ru—H bond strength in the same order. By applying the method developed by Tronconi and Lietti [41], we can estimate that the desorption energy of H* to about 31, 43 and 48 kcal/mol for RuM, RuMA and RuA, respectively.

In the case of RuA, the main desorption peak at 280 °C was followed by a secondary peak at higher temperature that, in line with previous similar reports [42,43], might be the result of more strongly adsorbed species.

N_2-TPD experiments did not reveal any appreciable nitrogen adsorption capacity.

3.3. Kinetic investigation

The activity and kinetic dependences of the three catalysts were measured at the GHSV of 20,000 $Nl/kg_{cat}/h$, within the temperature

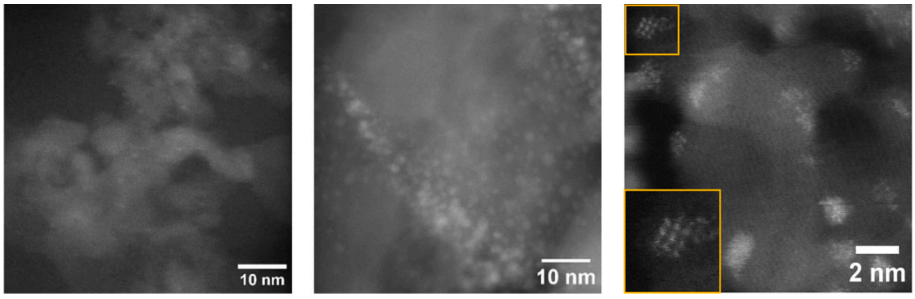

Fig. 1. HR-STEM image of a) RuA, b) RuM, c) RuMA.

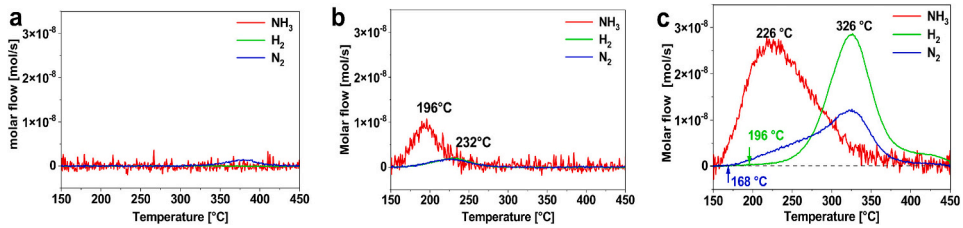

Fig. 4. NH_3, H_2 and N_2 molar flow during NH_3-TPD over a) RuM; b) RuMA; c) RuA.

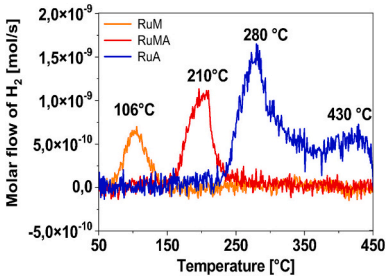

Fig. 5. Molar flow of H_2 over RuM, RuMA and RuA during H_2-TPD.

range of 240–500 °C, by exploring different feed compositions, to evaluate the effects of support, NH_3-inlet concentration and H_2/N_2 cofeeding. On purpose, NH_3 decomposition experiments were performed with catalyst bed dilution and large He-dilution to prevent any deviation from the isothermal behavior of the reactor. Only the cofeed of H_2 and N_2 was extended to large concentrations to bring the reacting system close to more representative conditions, as illustrated in Sections 3.3.1 and 3.3.2; still NH_3 concentration never exceeded 2.55 % to avoid axial and radial temperature gradients throughout the bed.

3.3.1. *Effect of supports*

Fig. 6 reports the results of NH_3 decomposition tests that were performed under 0.3 % and 2.55 % NH_3 in He to evaluate the effect of the nature of the supports. In each experiment, the stoichiometry of the reaction was verified by the independent measurement of NH_3, N_2 and H_2 molar flows; an example is reported in Fig. S4 in the Supplementary Material.

Surprisingly, the performance of RuM was fully comparable to that of RuA, despite the less favorable morphological properties and lower Ru dispersion. This seems to confirm the positive effect of basicity (also obtained in the literature by alkali doping) which apparently is also related to the strength of H* adsorption [44], here brought by MgO. Most studies have associated the promoting effect of basic components to the electron donating effect on Ru and a consequent favorable effect on the desorption of N* species [33]; here, the aforesaid H_2-TPD tests gave direct evidence that MgO favors the associative desorption of H* species.

The performance of RuMA was superior to that of the other systems, likely favored on one side by the basicity of the Mg-rich phase and on the other side by suitable morphological properties. The same relative order of activity was observed under all the operating conditions explored.

A more quantitative comparison among the formulations was addressed later in terms of intrinsic rate constants by the modelling analysis.

3.3.2. *Effects of feed composition*

Experiments were performed at increasing NH_3 concentration, and the results are reported in Fig. 7, panels a–c. For all the catalysts, NH_3 conversion decreased importantly at increasing inlet concentration. Additional experiments were performed where NH_3 concentration was kept constant and H_2 and N_2 were cofed. Experiments with 1–25 % H_2 co-feeding (panels d–f of Fig. 7) showed that the conversion curves shifted to progressively higher temperatures as hydrogen concentration increased, a clear evidence of strong hydrogen inhibition on NH_3 decomposition.

Analogous N_2 cofeed experiments were performed to evaluate possible coverage effects by nitrogen species. Fig. 8 compares the results of an experiment at 0.3 % NH_3 with and without N_2 co-feed: the measured NH_3 conversions were comparable. It was thus concluded that N_2 adsorption is negligible with respect to H_2 adsorption and does not influence the NH_3 cracking process, which is in line with independent results [34].

These observations are qualitatively consistent with previous reports in the literature (e.g. by Prasad et al. [45], who analyzed NH_3 decomposition over Ru/Al_2O_3 catalyst, with 0 %–40 % H_2 cofeeding). Differently from previous works, though, we further investigated the effect of varying NH_3 concentration at 25 % H_2-feed content, a condition that makes the kinetics insensitive to the quantity of H_2 produced by the reaction; the results are reported in Fig. 9 for the three formulations and show, in all cases, the overlap of the measured conversions. The manifest independence of NH_3 conversion on the reactant concentration clearly reveals that the reaction rate has a first order dependence on NH_3. This observation is in principle strictly related to the temperature range 400–480 °C, the same where conversion curves obtained at high

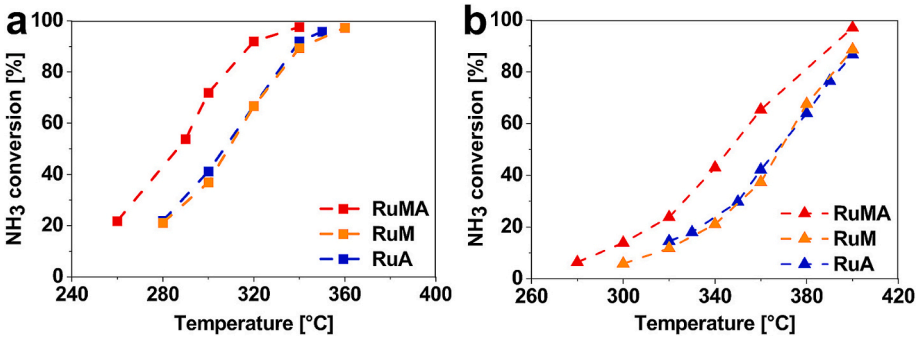

Fig. 6. NH_3 decomposition tests over RuMA (red line), RuM (yellow line), RuA (blue line). Operating conditions: GHSV =20,000 Nl /kg_{cat}/h; feed: a) 0.3 % NH_3 and b) 2.55 % NH_3. (For interpretation of the references to colour in this figure legend, the reader is referred to the web version of this article.)

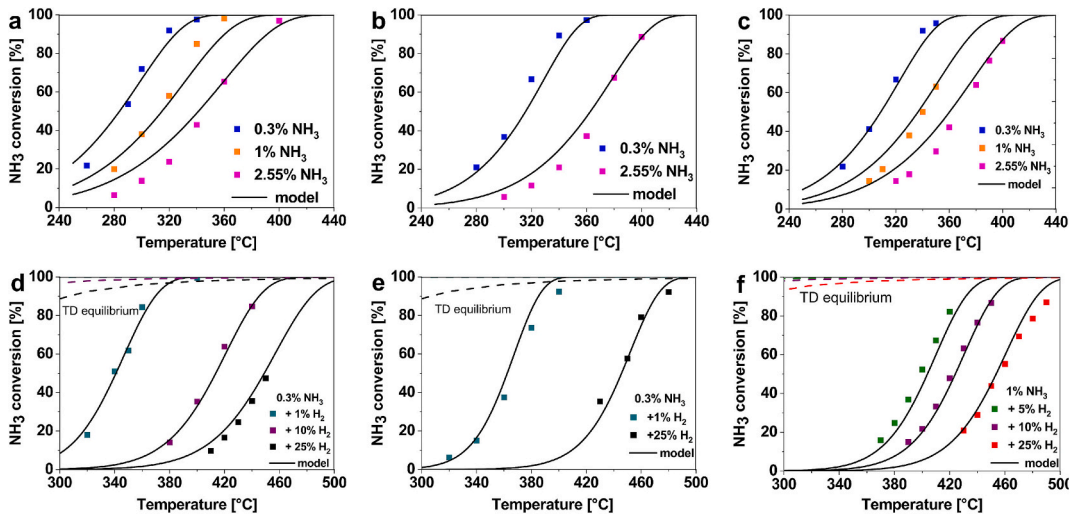

Fig. 7. Effect of NH_3-inlet concentration and H_2 cofeeding, a) & d) over RuMA; b) & e) over RuM; c) & f) over RuA. GHSV = 20,000 $Nl/kg_{cat}/h$. Symbols: experimental results; lines: modelling results.

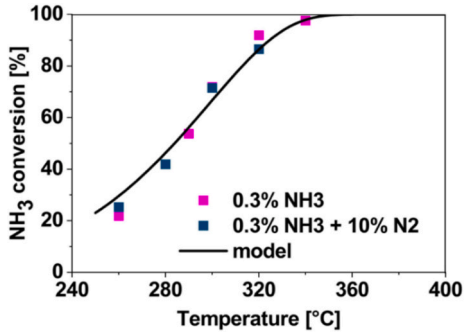

Fig. 8. Effect of N_2 co-feeding over RuMA. Symbols: experimental results; lines: modelling results.

ammonia concentration fall.

However, this original result has two major implications: (i) it suggests that even at lower temperatures, the NH_3 'self-inhibition' is an apparent effect, that can be partly explained by the hindering effect of hydrogen coverage; (ii) more importantly, it represents the direct evidence that ammonia activation is kinetically limiting under conditions representative of large H_2 concentrations, of interest for the industrial application.

Microkinetic analyses have already proposed that at increasing temperature the rate-determining step of NH_3 decomposition shifts from N* desorption to NH_2* dehydrogenation, based on theoretical evaluations on model Ru surfaces [46]. The data reported in Fig. 9 are, at the best of our knowledge, the first experimental evidence that indeed the rate-determining step is within the pattern of NH_3 dehydrogenation, in the temperature range of 280–480 °C. And that the same occurs for three supports, despite differences of basicity, morphology and Ru dispersion.

These results also provide a key for interpreting the relative activity of the three catalysts; in fact, based on the H_2-TPDs, an especially strong H* poisoning can be expected on RuA, while a much weaker tendency to surface H* saturation can be expected on RuM counterbalancing the lower Ru dispersion. Along the same lines, RuMA would be favored over RuA and RuM by large availability of Ru sites and intermediate H*-Ru energy.

It is herein very interesting to observe that analogous observations were obtained over a commercial Ru-based catalyst by Heraeus; Fig. S5 in the supplementary shows that the activity and the effects of feed composition measured over the commercial catalyst were comparable to the those of the home-made catalysts.

3.4. Kinetic modelling

The critical analysis of the collected data brings the authors to propose the following simple rate law as an adequate kinetic model, able to describe the key kinetic dependences avoiding the bias of parameter correlations:

$$r = k \bullet P_{NH_3} \Big/ P_{H_2}^{1.5} \tag{9}$$

The proposal is easily justified by the results of the cofeed experiments, that are reasonably believed mostly representative of realistic surface coverage conditions. The experiments reported in Fig. 9 give the direct evidence of first order dependence on NH_3 concentration in H_2-rich conditions, the H_2-cofeeding experiments in Fig. 7 reveal a negative order on H_2 concentration close to −1.5 and the N_2-cofeeding experiments reveal a zero-order dependence on N_2. Indeed, by adapting the simple power law model to the data, a very satisfactory description was obtained for all the catalysts as documented by the solid lines in

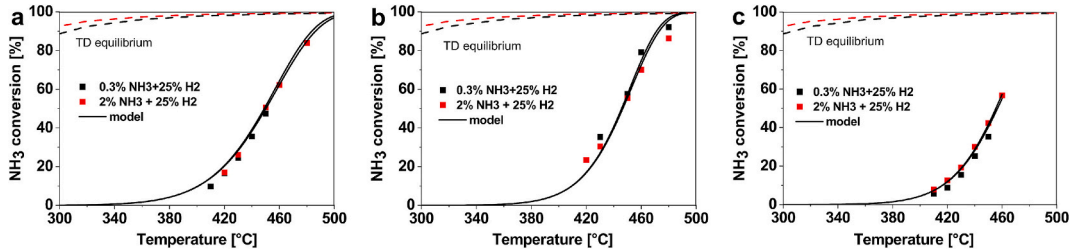

Fig. 9. Effect of NH_3-inlet concentration when co-feeding with 25 % H_2 over, a) RuMA; b) RuM; c) RuA. Symbols: experimental results; lines: modelling results.

Figs. 7–9.

Reaction orders adopted in Eq. (9) and the high model accuracy under H_2-rich conditions have a mechanistic interpretation, consistent with the literature [21]. Indeed, they can be easily obtained by assuming that: (i) the second dehydrogenation ($NH_2^* + * \rightarrow NH^* + H^*$) is the rate-determining step, (ii) the other steps are equilibrated and (iii) H* is the most abundant surface intermediate (MASI). Indicating with K_{NH3}, K_{H2} and K_{N2} the adsorption equilibrium constants of molecular species, K_1 the equilibrium constants for the first N—H cleavage, and k_2 the forward kinetic constant of the second N—H cleavage, we can easily obtain the following Langmuir Hinshelwood Hougen Watson type rate expression:

$$r = k_2 \bullet \left[NH_2^*\right] \bullet [*] = k_2 \bullet K_1 \bullet \frac{K_{NH_3}}{K_{H_2}^{0.5}} \bullet \frac{P_{NH_3}}{P_{H_2}^{0.5}} [*]^2 = k_2 \bullet K_1 \bullet \frac{K_{NH_3}}{K_{H_2}^{0.5}} \bullet \frac{P_{NH_3}}{P_{H_2}^{0.5}} \bullet \frac{1}{\left(1 + K_{NH_3} P_{NH_3} + K_{H_2}^{0.5} P_{H_2}^{0.5} + K_{N_2}^{0.5} P_{N_2}^{0.5}\right)^2} \quad (10)$$

where $\left[NH_2^*\right]$ and [*] represent the surface coverages of NH_2 adsorbed-species and free sites. The rate law (10) reduces then to the power law Eq. (9), with $k = k_2 \bullet K_1 \bullet \frac{K_{NH_3}}{K_{H_2}}$, under the assumption that the coverage of H* predominates over N*, adsorbed ammonia (and ammonia fragments) and free sites.

The proposed rate law (9) was adapted to the various datasets, for each catalyst; the Arrhenius temperature dependence of the apparent rate constant was rearranged in the following form:

$$k(T) = exp\left(ln\left(k\left(T_{ref}\right)\right) - \frac{E_{act}}{R} \bullet \left(\frac{1}{T} - \frac{1}{T_{ref}}\right)\right) \quad (11)$$

with reference temperature set at 600 K. The adaptive parameters $ln\left(k\left(T_{ref}\right)\right)$ and E_{act} were estimated for each catalyst and 95 % confidence limits were estimated based on the standard deviation among replicated experiments. The results are reported in Table 2.

A partial lack of accuracy of the simple power law model is noted in Fig. 7 by the prediction of the effect of ammonia inlet concentration at the lowest temperatures (here the relative error reaches in some cases values as high as 80–100 %, although the average absolute error is always within 6 %). Such inaccuracy can be attributed to the residual relevance of ammonia coverage that is accounted for in Eq. (10) and has been instead neglected in the reduced form of Eq. (9). Indeed, a very accurate description of the entire set of experiments can be obtained by adapting LHHW-type expressions, like Eq. (10), to the data; however, the estimated adsorption parameters are highly correlated, thus of no relevance for reactor considerations. It is herein important to observe that error introduced by the proposed rate law is limited to low temperatures and H_2-lean conditions and is the price of the model lumping, which is highly counterbalanced by the obtainment of robust, non-correlated parameter estimates, and the accurate description of the reaction dependences in the presence of H_2-rich reacting streams, of high relevance for the catalyst application.

The estimated rate constants are graphically represented in Fig. S6 in the Supplementary Material. Pre-exponential factors and temperature dependence are such that the scale of activity per unit mass of catalyst is in the order RuMA>RuA > RuM.

However, taking the measured CO/Ru ratio as a descriptor of Ru dispersion, the intrinsic activity per mole of exposed Ru appears in the order: RuMA>RuM≈RuA. This scale of reactivity is expected to represent at the best the effect of the nature of the support: it is thus well shown that MgO promotes the reactivity of the exposed Ru atoms more than Al_2O_3. Basicity of the support is thus a highly favoring factor. The spinel $MgAl_2O_4$ presents the best intrinsic activity per mole of exposed Ru and, remarkably, the lowest activation energy.

Considering the global nature of the estimated rate constant (proportional to the intrinsic rate of the second N—H cleavage and inversely proportional to the adsorption equilibrium constant of H_2), it is not possible to decouple the effect of the support on the energy barrier of the transition state (NH*-H*) from the effect on the strength of adsorption of hydrogen; however, the H_2-TPD experiments clearly showed that acidity is accompanied by more stable H* surface species, thus expectedly more important poisoning effect from H_2.

It is worthwhile further pointing out that the adoption of a simple power law model is not an oversimplification of the kinetic treatment; it is instead a very effective way to obtain robust and independent estimates of the kinetic parameters, as suitable for reactor design calculations. This consideration is not new in the literature; Gason and coworkers [4] have clearly shown that alternative mechanistic models based on different assumptions on the nature of the rate-determining step could describe comparably well the campaign of ammonia decomposition tests on a Ru-K/CaO catalyst obtained in the 1–40 bar pressure range; however, the result was obtained at the expense of several adaptive parameters. A power law model with fractional orders for NH_3 and H_2 (0.5 and − 1.2 respectively) resulted the most successful and rationale way to describe the observables. With respect to that reference study, herein we could push further the simplification of the kinetic model, since the unitary exponent for ammonia could be naturally deduced by the experiments at varying NH_3 concentration with large H_2 co-feed. As a consequence, we can conclude that the present data support the kinetic relevance of ammonia activation over the formulations studied; we cannot exclude that at lower temperatures desorption phenomena become rate controlling.

3.5. Implications of the kinetic dependences

The nature of the MASI and of the RDS explain the dramatic drop of reaction rates with increasing NH_3 concentration, such that under pure NH_3 feed, high conversions require very high temperatures (400 °C–550 °C) [24] and/or very low space velocities [42]; the use of high Ru loading has also been adopted in the literature (even 5 %) [6]. Before applying the power-law model to preliminary reactor calculations, the representativeness of the rate law was more stringently verified by the quantitative analysis of the data obtained over a commercial Heraeus catalyst, in the form of 1 mm beads. Fig. S7 shows the prediction of the effect of temperature and feed composition (effects of NH_3 and H_2-cofeed) up to the case of pure ammonia feed. A very satisfactory description of the data was obtained, which supports the intrinsic nature of the H_2-poisoning effect on Ru. This enforces that a kinetic investigation which explores a wide range of conditions, especially large H_2 cofeeding experiments, allows to train the kinetic modelling over a regime (high H* coverage) very similar to that experienced by the catalyst under pure ammonia.

The same data allows us to appreciate that a temperature rise of more than 100 °C is necessary to sustain ammonia conversion when passing

Table 2
Estimates of the kinetic parameters. T_{ref} = 600 K.

Parameters	ln(k(T_{ref}))	k(T_{ref})	$k_{Ru}(T_{ref})$	E_{ACT}	Average abs. Error
Unit	–	$\frac{mol_{NH_3}}{s \bullet g_{CAT}} \bullet atm^{0.5}$	$\frac{mol_{NH_3}}{s \bullet mol_{Ru}} \bullet atm^{0.5}$	$\frac{kcal}{mol}$	%
RuMA	−16.10 ±0.05	(9.90 ± 0.54) E-8	2.66E-05	38.0 ± 0.5	3.75
RuM	−17.78 ± 0.34	(1.89 ± 0.65) E-8	1.34E-05	50.7 ± 2.9	5.27
RuA	−17.39 ± 0.21	(2.81 ± 0.59) E-8	1.30E-05	45.6 ± 1.8	4.69

from a diluted ammonia feed to a concentrated one.

To better understand the reason behind this temperature shift, it is interesting to analyze how the reaction rate will evolve across an integral reactor. At this scope, Fig. 10 plots the calculated rate of NH_3 decomposition as a function of the extent of reaction for the case of Ru/$MgAl_2O_4$ catalyst, temperature of 400 °C, and different NH_3 inlet concentrations. At increasing consumption of the reactant and simultaneous progressive enrichment of the reacting stream with hydrogen, the reaction rate is subject to a dramatic drop; along an integral reactor, while conversion grows, the rate of the reaction will decrease by several orders of magnitude. Such a dramatic drop will result in a specular increase in the catalyst volume needed to raise the conversion. At increasing NH_3 feed content, the qualitative effect is maintained but the net values of reaction rates are lower, thus the catalyst volume needed to obtain a given conversion will need to grow.

The impact of these kinetic effects on the reactor sizing is highlighted in Fig. 11, where the simulations show the predicted effect of temperature at varying space velocity. Remarkably, it is observed that only by operating the reactor at GSHV<2500 Nl/kg_{cat}/h (thus with very large catalyst inventory), the complete conversion of ammonia will be obtained below 500 °C.

Furthermore, since the ammonia decomposition reaction occurs with increase of total number of moles, pressure has a negative impact on the calculated conversion at equilibrium; due to the negative reaction order, then, also the kinetics are disfavored by the increase of pressure. Indeed, a dedicated study by Gascon and coworkers [4] up to 40 atm has shown that the major impact of pressure is played within the 1–10 atm range.

These results highlight the importance of understanding the governing kinetic dependences and their impact on the operation of an integral reactor. In this respect, the strong interaction between the catalyst surface and the hydrogen produced during the reaction appears a major bottleneck to be addressed for favoring the technological deployment of ammonia decomposition.

The weakening of the Ru—H interaction emerges as a major objective for the development of improved catalyst formulations; the results herein presented show that enhanced electron donating properties of the support combined with suitable morphological properties are favorable features. At the reactor scale, the selective separation of H_2 can represent an effective strategy to mitigate such kinetic bottleneck even with conventional (and industrially reliable) catalyst formulations as those herein examined. Indeed, membrane reactors are being studied in literature [47]; experimental evidence has been provided on the enhancement of NH_3 conversion due to H_2 selective removal by Pd membranes or other H_2-selective membranes. The beneficial effect of integrating H_2 separation with reversible H_2 production processes is commonly associated with the thermodynamic effect of removing the reaction product; instead, in the case of ammonia decomposition on Ru-catalysts, the kinetic analysis herein presented allows to appreciate that an important benefit lies in intrinsic kinetics.

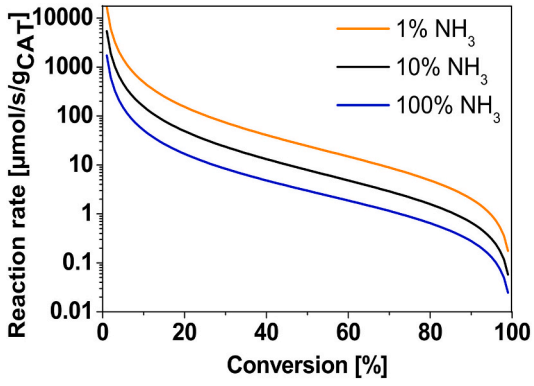

Fig. 10. Effect of the evolving composition of the reacting system on the reaction rate μ over RuMA, T = 400 °C. Feed composition: variable NH_3 inlet concentration with He complement.

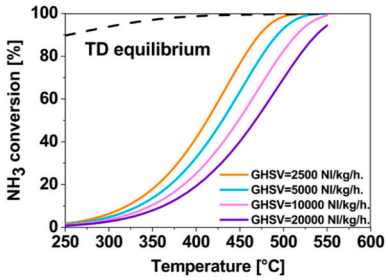

Fig. 11. Model prediction for effect of space velocity with pure NH_3 over RuMA.

4. Conclusions

In this work different Ru-based catalysts were studied to identify the major kinetic dependences of the ammonia decomposition reaction on Ru. Despite the wide literature on the topic and the unanimous evidence of apparent negative orders for NH_3 and H_2, the open debate on the nature of the controlling phenomena (i.e. nature of the RDS and identification of the MASI) prompted us to extend the kinetic investigation to cover unexplored crossed effects (effect of NH_3 concentration in the presence of H_2 cofeed) and dynamic experiments of adsorption/desorption of NH_3 and H_2. Besides, the experiments were performed under low concentrations of NH_3 to avoid any bias from temperature gradients across the catalytic bed and obtain rigorous kinetic evidence.

Over the three catalysts investigated, Ru/MgO, Ru/γ-Al_2O_3 and Ru/$MgAl_2O_4$, as well as over a commercial Ru-catalyst, the experiments under H_2-rich streams could be well described by a simple power-law rate expression (where the limited number of parameters excluded any correlation) with unitary order on NH_3 and order −1.5 on H_2. These orders are consistent with the hypothesis that H* is the MASI (that becomes stronger for the H_2-rich conditions) and the RDS is the $NH_2^* + * \rightarrow NH^* + H^*$ step. The two assumptions are internally consistent, since it is reasonable to expect that the second N—H cleavage becomes especially hindered in the presence of large H* coverage. It is also consistent with the evidence that the chemical and morphological properties of the support play a role in the energy of H* bonding, as inferred by the H_2-chemisorption experiments and the H_2-TPD. The same kinetic law shows instead some inaccuracy in describing the conversion at low temperature and H_2-lean conditions, where the adsorption/desorption of NH_3 or other species might become relevant. Still the assumed orders well explain the performance of a commercial catalyst from low to high NH_3 concentration.

The kinetic dependences are such that the progressive consumption of ammonia and the enrichment of hydrogen in the reacting steam is accompanied by a progressive dramatic decline of the reaction rate across the integral reactor, with a negative effect of feed concentration and total pressure. As a consequence, at the state of the catalyst performances assessed in this and other papers in the literature, high conversion of a pure NH_3 feed can be obtained below 500 °C only at very low space velocity. Still, the identification of the controlling kinetic phenomena (NH_3 activation and H* adsorption) provides guidelines towards improved catalyst formulations or more efficient reactor designs.

CRediT authorship contribution statement

Yi Qiu: Writing – original draft, Methodology, Investigation, Formal analysis, Data curation. **Federico Sascha Franchi:** Investigation, Data curation. **Nicola Usberti:** Writing – review & editing, Software, Investigation, Data curation. **Alessandra Beretta:** Writing – review & editing,

Supervision, Project administration, Conceptualization.

Declaration of competing interest

The authors declare that they have no known competing financial interests or personal relationships that could have appeared to influence the work reported in this paper.

Acknowledgements

The authors gratefully acknowledge financial support of this work via provision of a PhD scholarship to Yi Qiu by China Scholarship Council (CSC).

Appendix A. Supplementary data

Supplementary data to this article can be found online at https://doi.org/10.1016/j.fuproc.2025.108270.

Data availability

Data will be made available on request.

References

[1] K.E. Lamb, M.D. Dolan, D.F. Kennedy, Ammonia for hydrogen storage; a review of catalytic ammonia decomposition and hydrogen separation and purification, Int. J. Hydrog. Energy 44 (2019) 3580–3593, https://doi.org/10.1016/j.ijhydene.2018.12.024.

[2] M. Asif, S. Sidra Bibi, S. Ahmed, M. Irshad, M. Shakir Hussain, H. Zeb, M. Kashif Khan, J. Kim, Recent advances in green hydrogen production, storage and commercial-scale use via catalytic ammonia cracking, Chem. Eng. J. 473 (2023) 145381, https://doi.org/10.1016/j.cej.2023.145381.

[3] S. Mukherjee, S.V. Devaguptapu, A. Sviripa, C.R.F. Lund, G. Wu, Low-temperature ammonia decomposition catalysts for hydrogen generation, Appl. Catal. B 226 (2018) 162–181, https://doi.org/10.1016/j.apcatb.2017.12.039.

[4] S. Sayas, N. Morlanés, S.P. Katikaneni, A. Harale, B. Solami, J. Gascon, High pressure ammonia decomposition on Ru–K/CaO catalysts, Catal, Sci. Technol. 10 (2020) 5027–5035, https://doi.org/10.1039/d0cy00686f.

[5] https://www.portofrotterdam.com/en/news-and-press-releases/port-rotterdam-takes-important-step-making-shipping-more-sustainable-pilot.

[6] E. Spatolisano, L.A. Pellegrini, A.R. de Angelis, S. Cattaneo, E. Roccaro, Ammonia as a carbon-free energy carrier: NH_3 cracking to H_2, Ind. Eng. Chem. Res. 62 (2023) 10813–10827, https://doi.org/10.1021/acs.iecr.3c01419.

[7] https://www.topsoe.com/our-resources/knowledge/our-products/process-licensing/h2retake-process.

[8] J.C. Ganley, F.S. Thomas, E.G. Seebauer, R.I. Masel, A priori catalytic activity correlations: the difficult case of hydrogen production from ammonia, Catal. Lett. 96 (2004) 117–122, https://doi.org/10.1023/B:CATL.0000030108.50691.d4.

[9] I. Lucentini, X. Garcia, X. Vendrell, J. Llorca, Review of the decomposition of ammonia to generate hydrogen, Ind. Eng. Chem. Res. 60 (2021) 18560–18611, https://doi.org/10.1021/acs.iecr.1c00843.

[10] Z. Zaidi, Y. Kamlesh, S. Gupta, M. Mudgal Singhai, A. Singh, Emerging trends in research and development on earth abundant materials for ammonia degradation coupled with H_2 generation, Sci. Technol. Adv. Mater. 25 (2024) 2301423, https://doi.org/10.1080/14686996.2023.2301423.

[11] A.M. Karim, V. Prasad, G. Mpourmpakis, W.W. Lonergan, A.I. Frenkel, J.G. Chen, D.G. Vlachos, Correlating particle size and shape of supported $Ru/\gamma\text{-}Al_2O_3$ catalysts with NH_3 decomposition activity, J. Am. Chem. Soc. 131 (2009) 12230–12239, https://doi.org/10.1021/ja902587k.

[12] H.B. Kim, E.D. Park, Ammonia decomposition over Ru catalysts supported on alumina with different crystalline phases, Catal. Today 411–412 (2023) 113817, https://doi.org/10.1016/j.cattod.2022.06.032.

[13] S.F. Yin, B.Q. Xu, X.P. Zhou, C.T. Au, A mini-review on ammonia decomposition catalysts for on-site generation of hydrogen for fuel cell applications, Appl. Catal. A Gen. 277 (2004) 1–9, https://doi.org/10.1016/j.apcata.2004.09.020.

[14] S.F. Yin, Q.H. Zhang, B.Q. Xu, W.X. Zhu, C.F. Ng, C.T. Au, Investigation on the catalysis of CO_x-free hydrogen generation from ammonia, J. Catal. 224 (2004) 384–396, https://doi.org/10.1016/j.jcat.2004.03.008.

[15] E. Fu, Y. Qiu, H. Lu, S. Wang, L. Liu, H. Feng, Y. Yang, Z. Wu, Y. Xie, F. Gong, R. Xiao, Enhanced NH_3 decomposition for H_2 production over bimetallic M (M=Co, Fe, Cu) Ni/Al_2O_3, Fuel Process. Technol. 221 (2021) 106945, https://doi.org/10.1016/j.fuproc.2021.106945.

[16] A. Di Carlo, L. Vecchione, Z. Del Prete, Ammonia decomposition over commercial Ru/Al_2O_3 catalyst: an experimental evaluation at different operative pressures and temperatures, Int. J. Hydrog. Energy 39 (2014) 808–814, https://doi.org/10.1016/j.ijhydene.2013.10.110.

[17] J. Zhang, H. Xu, Q. Ge, W. Li, Highly efficient Ru/MgO catalysts for NH_3 decomposition: synthesis, characterization and promoter effect, Catal. Commun. 7 (2006) 148–152, https://doi.org/10.1016/j.catcom.2005.10.002.

[18] X. Ju, L. Liu, X. Zhang, J. Feng, T. He, P. Chen, Highly efficient Ru/MgO catalyst with surface-enriched basic sites for production of hydrogen from ammonia decomposition, ChemCatChem 11 (2019) 4161–4170, https://doi.org/10.1002/cctc.201900306.

[19] D. Szmigiel, W. Raróg-Pilecka, E. Miśkiewicz, Z. Kaszkur, Z. Kowalczyk, Ammonia decomposition over the ruthenium catalysts deposited on magnesium–aluminum spinel, Appl. Catal. A Gen. 264 (2004) 59–63, https://doi.org/10.1016/j.apcata.2003.12.038.

[20] A. Hellman, E.J. Baerends, M. Biczysko, T. Bligaard, C.H. Christensen, D.C. Clary, S. Dahl, R. Van Harrevelt, K. Honkala, H. Jonsson, G.J. Kroes, M. Luppi, U. Manthe, J.K. Nørskov, R.A. Olsen, J. Rossmeisl, E. Skúlason, C.S. Tautermann, A.J. C. Varandas, J.K. Vincent, Predicting catalysis: understanding ammonia synthesis from first-principles calculations, J. Phys. Chem. B 110 (2006) 17719–17735, https://doi.org/10.1021/jp056982h.

[21] A.B. Mhadeshwar, J.R. Kitchin, M.A. Barteau, D.G. Vlachos, The role of adsorbate–adsorbate interactions in the rate controlling step and the most abundant reaction intermediate of NH_3 decomposition on Ru, Catal. Lett. 96 (2004) 13–22, https://doi.org/10.1023/B:CATL.0000029523.22277.e1.

[22] Y. Wang, M.R. Kunz, Z. Fang, G. Yablonsky, R. Fushimi, Accumulation dynamics as a new tool for catalyst discrimination: an example from ammonia decomposition, Ind. Eng. Chem. Res. 58 (2019) 10238–10248, https://doi.org/10.1021/acs.iecr.9b01470.

[23] C. Qin, S. Ruan, C. He, L. Zhang, Nickel perovskite catalysts for ammonia decomposition: DFT calculations and microreaction kinetics, Colloids Surf. A Physicochem. Eng. Asp. 691 (2024) 133898, https://doi.org/10.1016/j.colsurfa.2024.133898.

[24] L. Yu, F. Abild-Pedersen, Bond order conservation strategies in catalysis applied to the NH_3 decomposition reaction, ACS Catal. 7 (2017) 864–871, https://doi.org/10.1021/acscatal.6b03129.

[25] D.A. Hansgen, D.G. Vlachos, J.G. Chen, Using first principles to predict bimetallic catalysts for the ammonia decomposition reaction, Nat. Chem. 2 (2010) 484–489, https://doi.org/10.1038/nchem.626.

[26] T. Su, B. Guan, J. Zhou, C. Zheng, J. Guo, J. Chen, Y. Zhang, Y. Yuan, W. Xie, N. Zhou, H. Dang, B. Xu, Z. Huang, Review on Ru-based and Ni-based catalysts for ammonia decomposition: research status, reaction mechanism, and perspectives, Energy Fuel 37 (2023) 8099–8127, https://doi.org/10.1021/acs.energyfuels.3c00804.

[27] S.R. Logan, C. Kemball, The catalytic decomposition of ammonia on evaporated metal films, Trans. Faraday Soc. 56 (1960) 144–153, https://doi.org/10.1039/TF9605600144.

[28] A. Takahashi, T. Fujitani, Kinetic analysis of decomposition of ammonia over Nickel and Ruthenium catalysts, J. Chem. Eng. Jpn 49 (2016) 22–28, https://doi.org/10.1252/jcej.14we431.

[29] H. Fang, D. Liu, Y. Luo, Y. Zhou, S. Liang, X. Wang, B. Lin, L. Jiang, Challenges and opportunities of Ru-based catalysts toward the synthesis and utilization of ammonia, ACS Catal. 12 (2022) 3938–3954, https://doi.org/10.1021/acscatal.2c00090.

[30] H. Liu, Y. Zhang, S. Liu, S. Li, G. Liu, $Ni\text{-}CeO_2$ nanocomposite with enhanced metal-support interaction for effective ammonia decomposition to hydrogen, Chem. Eng. J. 473 (2023) 145371, https://doi.org/10.1016/j.cej.2023.145371.

[31] S.R. Kulkarni, N. Realpe, A. Yerrayya, V.K. Velisoju, S. Sayas, N. Morlanes, J. Cerillo, S.P. Katikaneni, S.N. Paglieri, B. Solami, J.P. Castaño, Elucidating the rate-determining step of ammonia decomposition on Ru-based catalysts using ab initio-grounded microkinetic modeling, Cat. Sci. Technol. 13 (2023) 2026, https://doi.org/10.1039/d3cy00055a.

[32] G. Lezcano, N. Realpe, S.R. Kulkarni, S. Sayas, J. Cerrillo, N. Morlanes, H. O. Mohamed, V.K. Velisoju, R.F. Aldilajan, S.P. Katikaneni, M. Rakib, B. Solami, J. Gascon, P. Castaño, Unraveling the promoter role of Ba in Co–Ce catalysts for ammonia decomposition using microkinetic modeling, Chem. Eng. J. 471 (2023) 144623, https://doi.org/10.1016/j.cej.2023.144623.

[33] Z. Wang, Z. Cai, Z. Wei, Highly active ruthenium catalyst supported on barium hexaaluminate for ammonia decomposition to CO_x-free hydrogen, ACS Sustain. Chem. Eng. 7 (2019) 8226–8235, https://doi.org/10.1021/acssuschemeng.8b06308.

[34] Z. Su, J. Guan, Y. Liu, D. Shi, Q. Wu, K. Chen, Y. Zhang, H. Li, Research progress of ruthenium-based catalysts for hydrogen production from ammonia decomposition, Int. J. Hydrog. Energy 51 (2024) 1019–1043, https://doi.org/10.1016/j.ijhydene.2023.09.107.

[35] J. Perez-Ramirez, R.J. Berger, G. Mul, F. Kapteijn, J.A. Moulijn, The six-flow reactor technology: A review on fast catalyst screening and kinetic studies, Catal. Today 60 (2000) 93–109, https://doi.org/10.1016/S0920-5861(00)00321-7.

[36] L.J. Gillespie, J.A. Beattie, The thermodynamic treatment of chemical equilibria in systems composed of real gases. I. An approximate equation for the mass action function applied to the existing data on the haber equilibrium, Phys. Rev. 36 (1930) 743, https://doi.org/10.1103/PhysRev.36.743.

[37] G. Bergeret, P. Gallezot, Handbook of heterogenous catalysis, 2, Wiley-VCH 10 (2008) 738–765, https://doi.org/10.1002/9783527610044.hetcat0038.

[38] J. Feng, N. Wan, X. Ju, L. Liu, L. Bai, X. Zhao, T. He, Efficient Ru/Y_2O_3 catalyst derived from Ru nanoparticles on yttrium carbonate for production of hydrogen from ammonia decomposition, ChemCatChem (2024) e202401314, https://doi.org/10.1002/cctc.202401314.

[39] S. Gong, Z. Du, Y. Tang, J. Chen, Encapsulation of Ru nanoparticles within NaY zeolite for ammonia decomposition, Int. J. Hydrog. Energy 88 (2024) 142–150, https://doi.org/10.1016/j.ijhydene.2024.09.178.
[40] X. Guo, Y. Li, R. Shi, Q. Liu, E. Zhan, W. Shen, Co/MgO catalysts for hydrogenolysis of glycerol to 1, 2-propanediol, Appl. Catal. A Gen. 371 (2009) 108–113, https://doi.org/10.1016/j.apcata.2009.09.037.
[41] E. Tronconi, L. Lietti, An exact single-curve analysis technique for TPD spectra, Surf. Sci. 199 (1988) 43–53, https://doi.org/10.1016/0039-6028(88)90395-0.
[42] Q. Su, L.L. Gu, A.H. Zhong, Y. Yao, W.J. Ji, W.P. Ding, C.T. Au, Layered double hydroxide derived Mg_2Al-LDO supported and K-modified Ru catalyst for hydrogen production via ammonia decomposition, Catal. Lett. 148 (2018) 894–903, https://doi.org/10.1007/s10562-017-2195-1.
[43] H. Fang, S. Wu, T. Ayvali, J. Zheng, J. Fellowes, P.L. Ho, K.C. Leung, A. Large, G. Held, R. Kato, K. Suenaga, Y.I.A. Reyes, H.V. Thang, H.Y.T. Chen, S.C.E. Tsang, Dispersed surface Ru ensembles on MgO(111) for catalytic ammonia decomposition, Nat. Commun. 14 (2023) 647, https://doi.org/10.1038/s41467-023-36339-w.
[44] C. Chen, K. Wu, H. Ren, C. Zhou, Y. Luo, L. Lin, C. Au, L. Jiang, Ru-based catalysts for ammonia decomposition: a mini-review, Energy Fuel 35 (2021) 11693–11706, https://doi.org/10.1021/acs.energyfuels.1c01261.
[45] V. Prasad, A.M. Karim, A. Arya, D.G. Vlachos, Assessment of overall rate expressions and multiscale, microkinetic model uniqueness via experimental data injection: ammonia decomposition on Ru/γ-Al_2O_3 for hydrogen production, Ind. Eng. Chem. Res. 48 (2009) 5255–5265, https://doi.org/10.1021/ie900144x.
[46] W. Tsai, W.H. Weinberg, Steady-state decomposition of ammonia on the Ru(001) surface, J. Phys. Chem. 91 (1987) 5302–5307. https://pubs.acs.org/sharinguidelines.
[47] V. Cechetto, L. Di Felice, F. Gallucci, Advances and perspectives of H_2 production from NH_3 decomposition in membrane reactors, Energy Fuel 37 (2023) 10775–10798, https://doi.org/10.1021/acs.energyfuels.3c00760.